Geology, Geophysics & Environment 2025, vol. 51 (1): 89–100

Alpha particle distribution and uranium mechanisms of accumulation in fossilised shells of ammonites and bivalves

Magdalena Długosz-Lisiecka[1], Dagmara Tchorz-Trzeciakiewicz[2]

[1] *Lodz University of Technology, Faculty of Chemistry, Institute of Applied Radiation Chemistry, Łódź, Poland, ORCID ID: 0000-0003-1358-049X*
[2] *University of Wrocław, Institute of Geological Sciences, Wrocław, Poland, e-mail: dagmara.tchorz-trzeciakiewicz@uwr.edu.pl (corresponding author), ORCID ID: 0000-0001-6938-8881*

Received: 9 August 2024; accepted: 21 March 2025; first published online: 30 March 2025

Abstract: The uranium concentration and distribution in fossils (ammonite and bivalve specimens) were studied. Fossil samples were cut perpendicularly and thin sections were prepared. The chemical and mineralogical compositions of fossils were analysed using scanning electronic microscopy (SEM) with energy-dispersive X-ray spectroscopy (EDS). The distribution of alpha emitters in the area of fossils was registered using CR-39 detectors. Alpha particle emitters were almost evenly distributed in all analysed fossils. We do not observe tracks concentrated in specific regions, which may indicate the absence of highly radioactive mineral grains. The uniformly distributed alpha tracks correlated with areas of mineral composition dominated by apatite, $Ca_5(PO_4)_3(Cl/F/OH)$. The correlation between phosphorous content and alpha tracks suggests that this element was crucial in absorbing radionuclides, presumably uranium or other alpha particle emitters, uranium progenies. However, upon analysing the chemical composition on thin sections of fossils, uranium was not detected, likely due to its concentrations being below the detection limits of EDS. Areas on the thin sections devoid of alpha tracks on CR-39 detectors were associated with empty voids in thin sections, ooids partially composed of FeS_2 (pyrite framboids) or iron oxides F_2O_3 (hematite), phosphorus-free regions, or other areas where crushed fragments of shells composed of calcium carbonate (aragonite) partially filled internal casts. The interaction of elements presented in fossil structures with uranium can depend on various factors, such as the pH of the pore fluids, redox conditions, and the specific mineralogy of the sediments. Our research indicates that the increased radioactivity registered in some fossils is connected with phosphorous content. Small amounts of uranium are disseminated in calcium phosphate (various apatite forms). The uranium concentrations smaller than the detection limit of EDS can be successfully registered using passive track detectors.

Keywords: uranium, alpha emitters, fossil record, fossilization, phosphatization, radioactivity

INTRODUCTION

The influence of organic compounds in vertebrate and invertebrate fossils on uranium concentration is poorly understood and remains an area of ongoing research. In some fossils, higher concentrations of uranium can be observed due to uranium uptake (Długosz-Lisiecka et al. 2021). Uranium is a naturally occurring radioactive element found in rocks and soils that can be dissolved in water. The content in the Earth's crust is from 0.9 mg/kg to 2.8 mg/kg (Hu & Gao 2008), but in the sediments of the Karelian lakes, the values varied between 0.14 mg/kg and 42.33 mg/kg (Slukovskii 2023).

In most cases, the geology and geochemistry studies of the various areas showed that the rocks or sediments with a high uranium content have elevated concentrations of thorium, which often accompanies uranium. Uranium exists in two oxidation states in the environment: U(VI) soluble and U(IV) insoluble in water.

Sedimentary ore deposits typically form when uranium dissolved in groundwater encounters reducing conditions, causing it to precipitate as "pitchblende" (uraninite, UO_2) (Mustoe 2020). In these conditions, uranium is relatively soluble and can be transported by groundwater. When groundwater comes into contact with buried organic structures over thousands of years, uranium can leach into the fossilised material without Th. In reducing conditions, U(VI) is altered to U(IV) and precipitates as insoluble uranium minerals.

Several main factors contribute to the higher uranium concentration in fossils – shells of cephalopods, corals and bones, including environmental conditions, fossilisation process, microporosity and mineral composition (e.g. calcium carbonates, calcium phosphate, iron or manganese oxides) (Tan et al. 2007, Wang et al. 2019).

The geological and hydrological conditions of sites where fossils of ancient organisms are buried play a significant role in uranium uptake. If the area has high levels of uranium in the surrounding rocks and soil, there is a greater chance of uranium being present in the water that comes into contact with bones (Zhao et al. 2012, Cid et al. 2014). Over time, this can lead to uranium accumulation within the structure of buried organisms remains. The burial conditions, such as the burial depth, temperature, and groundwater flow, can also affect the degree of uranium uptake. Vertebrate and invertebrate fossils can be buried for thousands or even millions of years, allowing uranium to accumulate. The longer the fossil remains buried, the more time elements accumulate within the bone structure, including uranium. Length of the fossilisation process can significantly impact the final concentration of uranium in the fossil (Dahl et al. 2021).

The processes of uranium uptake in fossils can be influenced by the initial composition of the elements and compounds in the fossils themselves. Fossils that contain many organic materials, such as petrified wood or the remains of organisms, may act as preferential uranium accumulation sites (Mustoe 2020). That's because organic materials often have a strong affinity for uranium compounds, and their presence may favour the concentration of this element in specific areas of fossils (Zhang et al. 2020, Długosz-Lisiecka et al. 2021).

Jiménez-Arroyo et al. (2023) show that phosphate minerals, such as apatite, have a strong affinity for uranium and can preferentially react with and incorporate uranium into their crystal structure during diagenesis. Apatite is common in fossilised bones and can influence the uranium concentration in these fossils (Trueman & Tuross 2002, Długosz-Lisiecka et al. 2021). The sorption of uranium using phosphates primarily involves surface complexation and ion exchange mechanisms. Phosphate minerals, such as apatite, have a high affinity for uranium and can preferentially sorb uranium ions (U^{6+}) onto their surfaces (Boukhenfouf & Boucenna 2012). Phosphate minerals have negatively charged surfaces due to phosphate groups (PO_4^{3-}) in their crystal lattice. As a cation (U^{6+}), uranium can form strong surface complexes with these negatively charged phosphate groups. The surface complexation involves the electrostatic attraction between the positively charged uranium ions and the negatively charged phosphate mineral surface. This process allows uranium to adsorb onto the phosphate mineral, effectively concentrating uranium in the solid phase. The surface complexation mechanism is fundamental in neutral to alkaline pH conditions, where the phosphate mineral surfaces are negatively charged and capable of forming strong surface complexes with uranium (Constantin et al. 2022, Clarkson et al. 2023, Lan et al. 2024).

When uranium is complexed on phosphates, various chemical compounds can form depending on the specific phosphate mineral and the complexation conditions (Deng et al. 2023). The most common complex formed is the surface complex between uranium (U^{6+}) and the negatively charged phosphate groups (PO_4^{3-}) in the crystal lattice of phosphate minerals. This surface complex is essential for sorbing uranium onto the

phosphate mineral surfaces. The specific chemical formula for this surface complex can vary, but it is generally represented as follows:

$$UO_2(HPO_4)^{2-} \text{ or } UO_2(PO_4)^{2-} \quad (1)$$

In this surface complex, the uranium ion (U^{6+}) is coordinated with two or more phosphate groups. The exact coordination and geometry of the complex depend on the structure of the phosphate mineral and the environmental conditions (Skomurski et al. 2011, Cid et al. 2014, Moyo et al. 2014).

Additionally, when uranium is sorbed onto phosphate minerals, it may form inner-sphere or outer-sphere complexes (Bruneton et al. 2014). In inner-sphere complexes, the uranium ion is directly bonded to the oxygen atoms in the phosphate groups. In contrast, in outer-sphere complexes, the uranium ion is adsorbed on the mineral surface through electrostatic forces without direct bonding. Apart from these surface complexes, uranium can also form secondary minerals or solid phases in the presence of phosphates. For example, under specific conditions, uranyl phosphate minerals like autunite ($Ca(UO_2)_2(PO_4)_2{\cdot}10–12H_2O$) or meta-autunite ($Ca(UO_2)_2(PO4)_2{\cdot}6H_2O$) can precipitate from solution when uranium is in the presence of calcium and phosphate ions.

The nature of the chemical compounds formed when uranium complexes on phosphates vary based on the specific phosphate mineral, uranium concentration and other ions in the solution, pH, temperature, and other environmental factors. Complexation of uranium with phosphates can change for various applications, including the immobilisation of uranium in waste management and the study of uranium behaviour in the environment and geological formations. Phosphate minerals can exchange ions with other cations in the surrounding solution, including natural radionuclides. In ion exchange, the positively charged uranium ions replace other cations (e.g., calcium, sodium) loosely bound to the surface of the phosphate mineral. The ion exchange mechanism can be significant when the concentration of other cations in the solution is high, providing more opportunities for exchanging uranium onto the mineral surfaces (IAEA 2009, Reynolds et al. 2018, Zhang et al. 2020, Rasbury et al. 2023, Hatje et al. 2024).

The study aims to analyse the distribution of alpha-radiation emitting elements in selected fossils of ammonites and bivalves, which are characterised by increased radioactivity. Additionally, an effort was made to examine the processes of uranium accumulation and the mechanisms underlying it in sedimentary environments. Significant part of these studies is the analysis of processes of uranium accumulation and its mechanisms in sediment environments.

MATERIAL AND METHODS

The fossils utilised in our research are sourced from the collection housed at the Geologic Museum at the University of Lodz. The samples originate from a single location, Pulnoy in France, from the Jurassic period.

The radioactivity of analysed fossils, including ^{238}U, ^{235}U, ^{228}Ac and ^{40}K, was assessed by Długosz-Lisiecka et al. (2021) using a gamma spectrometry system. The samples were analysed by a low-background gamma-ray spectrometry system based on the HPGe detector of model GX3020, with a relative efficiency equal to 30% (Canberra). A unique system with an anticoincidence shield is located at the Lodz University of Technology at the Institute of Applied Radiation Chemistry in the Isotope Methods Laboratory (Długosz-Lisiecka 2016). Each measurement was conducted over an average time of 80,000 s, resulting in measurement uncertainties not exceeding 10%. For ^{238}U isotope analysis of radioactive isotope activity, average activity concentrations of ^{234}Th (63.3 keV) and ^{234m}Pa (1001 keV) were applied (Fig. 1). ^{235}U isotope concentration has been analysed based on a 143.7 keV peak energy line. The characteristics of each fossil and each sample's dose rate are given in Table 1.

All fossil samples were cut perpendicularly, and thin sections were prepared. The chemical and mineralogical compositions of fossils were analysed using scanning electronic microscopy (SEM) with energy dispersive X-ray spectroscopy (EDS) SEM Jeol JSM-IT500LA (landing voltage 25 kV).

The distribution of alpha-emitting radionuclides on thin sections of fossils was evaluated based on the spatial distribution of alpha particle impact traces (black tracks) on the surface of CR-39 detectors. The CR-39 detectors (passive track detectors) were affixed to thin sections for 9 months. The detectors were etched in 6M NaOH at 60°C after exposure. During this procedure, the alpha particle impact traces were enlarged to the size that allowed them to be observed under a microscope. The distribution of alpha particle traces was examined under the Zeiss Axio Imager Z2 microscope.

The use of autoradiography to determine the distribution of radionuclides in rocks and minerals employing alpha track detectors has a long tradition. The use of CR-39 detectors was proposed by Ochmann and Solecki (2005). The hits of alpha particles damage the material's atomic lattice, producing a disintegration track. Etching in a preferential solution causes the traces to become enlarged, allowing it to be easily viewed using a microscope.

The alpha decay of ^{238}U gives rise to another alpha-emitting descendants: ^{234}U, ^{230}Th, ^{226}Ra, ^{222}Rn, ^{218}Po, ^{214}Po and ^{210}Po. Similarly, the alpha-decay of ^{235}U (which comprises 0.72% of natural uranium) produces the following alpha-emitting descendants: ^{231}Pa, ^{233}Ra, ^{219}Rn, ^{215}Po, ^{211}Bi, ^{211}Po. The alpha particle emitter is also ^{232}Th, and some decay products include ^{228}Th, ^{224}Ra, ^{220}Rn, ^{216}Po and ^{212}Po.

RESULTS AND DISCUSSION

Preliminary gamma radiation measurements indicated the presence of uranium isotopes ^{235}U and ^{238}U, along with several of their natural progenies (Fig. 1). The variation in the ^{238}U/^{235}U activity ratio in natural samples is typically expected to be around 21.7. The oxidation or reduction process may slightly favour one isotope over the other. Natural uranium deposits are not always uniform. Variations in the local geology or mineralogy might lead to differences in the ratio; therefore, in this study, we observed slight changes between 20.0 and 22.1 (Table 1).

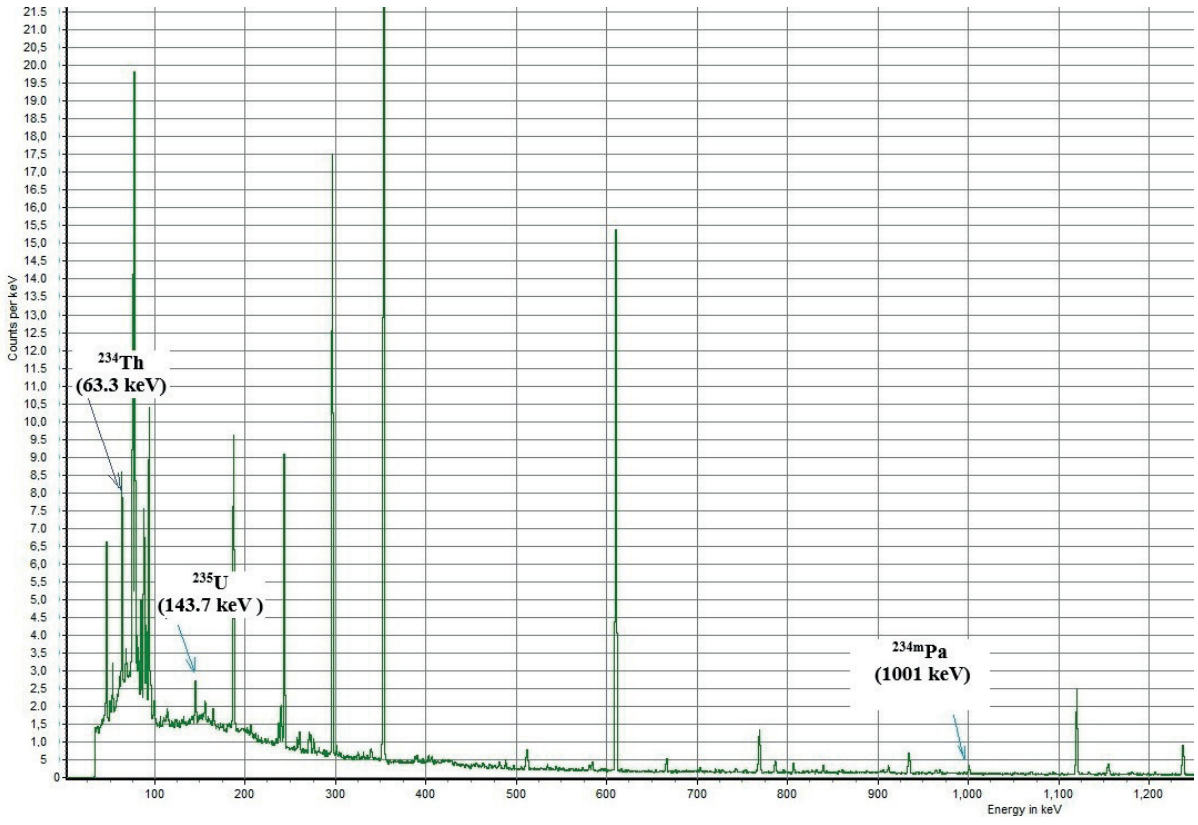

Fig. 1. *Spectrum of gamma radiation with ^{234}Th (63.3 keV) and ^{234m}Pa (1001 keV) as ^{238}U progenies and ^{235}U (143.7 keV)*

Table 1
^{238}U and ^{235}U isotope content in fossil samples

ID	Name of sample		Age	^{238}U concentration [Bq/kg]	^{235}U concentration [Bq/kg]
	type of fossil	systematic position			
CP MDL 0001	ammonite	Ammonoidea, *Arietites* sp.	Lower Jurassic (Sinemurian)	830 ±33	38 ±5
CP MDL 0003	bivalve	Ostreida, *Gryphaea dilatata*	Upper Jurassic (Oxfordian/ Kimmeridgian)	419 ±25	19 ±3
CP MDL 0004	bivalve	genus and species unspecified	unknown	610 ±45	30 ±6
CP MDL 0007	ammonite	Ammonoidea *Haugia variabilis*	Lower Jurassic (Toarcian)	327 ±25	16 ±2
CP MDL 0009	bivalve	Limida, *Plagiostoma* sp.	Lower Jurassic	1201 ±92	60 ±14

The thin sections made from fossils were analysed under a microscope. The internal structure of ammonites is visible, such as chambers divided by seams CP MDL 0007 or septa CP MDL 001 composed of calcium carbonate (aragonite). The chambers are filled with sediments with microfossils. In the case of bivalves, we can notice sediments which fill the inside of their shells. The bivalve shell, composed of aragonite, is preserved only in one specimen CP MDL 0003).

The presence of alpha emitters was confirmed using passive track detectors CR-39. The distribution of alpha tracks (black tracks) in all analysed samples is relatively homogenous, which may indicate the absence of highly radioactive mineral grains (Fig. 2). The presence of such grains is demonstrated by highly concentrated and high-density track clusters.

The uniformly distributed alpha tracks correlate with areas of mineral composition dominated by apatite, $Ca_5(PO_4)_3(Cl/F/OH)$, usually with minor admixtures of submicroscopic silicates, probably clay minerals (Fig. 3A, C, D) and sodic feldspar (Fig. 3B). Some amount of Fe detected in these areas is most likely due to dispersed Fe oxides-hydroxides. Areas devoid of alpha tracks are associated with empty voids in thin sections (Fig. 4C – on the interleaf), ooides partially composed of FeS_2 (pyrite framboids) (Fig. 4B) ooides composed of Fe oxides (hematite) (Fig. 4D), or phosphorus-free areas (Fig. 4A) or other areas where crushed fragments of shells partially filled internal cast (Fig. 2A–C). We suggest that the contents of uranium and thorium, elements responsible for the emission of alpha particles, are below the detection limits of EDS and were not measured. The good positive correlation between phosphorus content and alpha tracks indicates that this element was crucial in absorbing radionuclides, presumably uranium or other alpha particle emitters, uranium progenies.

The phosphorous minerals were present in the fillings of the bivalves and ammonites (Fig. 2A). In marine settings, phosphorus is naturally sourced from nutrient runoff via weathering and oceanic upwelling. Enriched phosphate content in sediments can be caused by:

- basin-scale process that affects P availability,
- burial of phosphate absorbed onto iron oxide particulates,
- remineralisation of phosphate from organic matter through microbial respiration, or other microbial activities (such as storage and release of phosphates) that influence porewater chemistry.

Phosphogenesis is often driven by microbial sulphate reduction and the reduction of iron oxide particulates. These particulates play a critical role in limiting phosphate diffusion from sediments to bottom waters through a process called "iron-pumping."

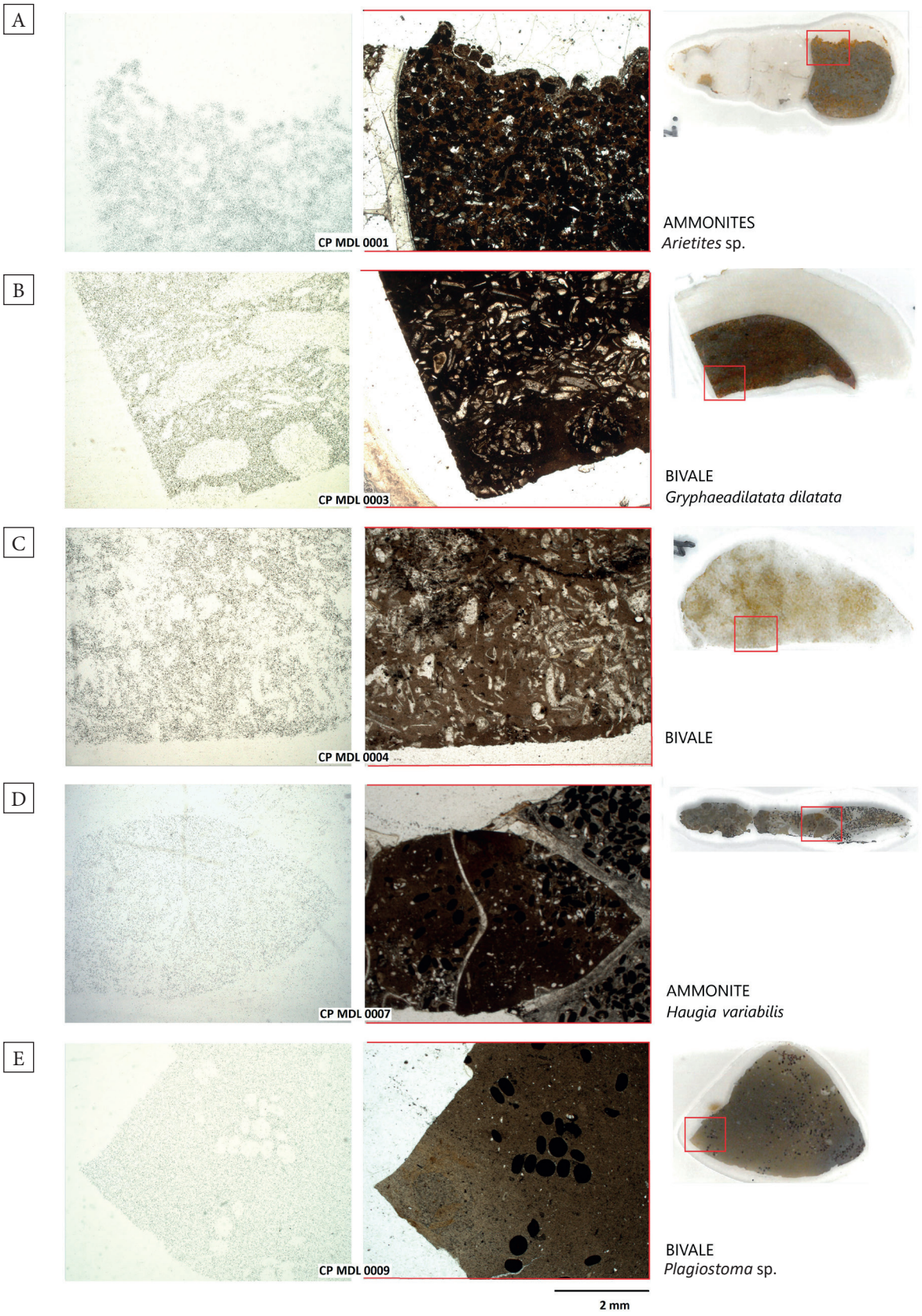

Fig. 2. *The compilation of the thin section and CR-39 detectors. Shells and internal cast of ammonites and bivalves: A) ammonite (Arietites sp.); B) bivalve (Gryphaea dilatata); C) bivalve (unspecified); D) ammonite (Haugia variabilis); E) bivalve (Plagiostoma sp.)*

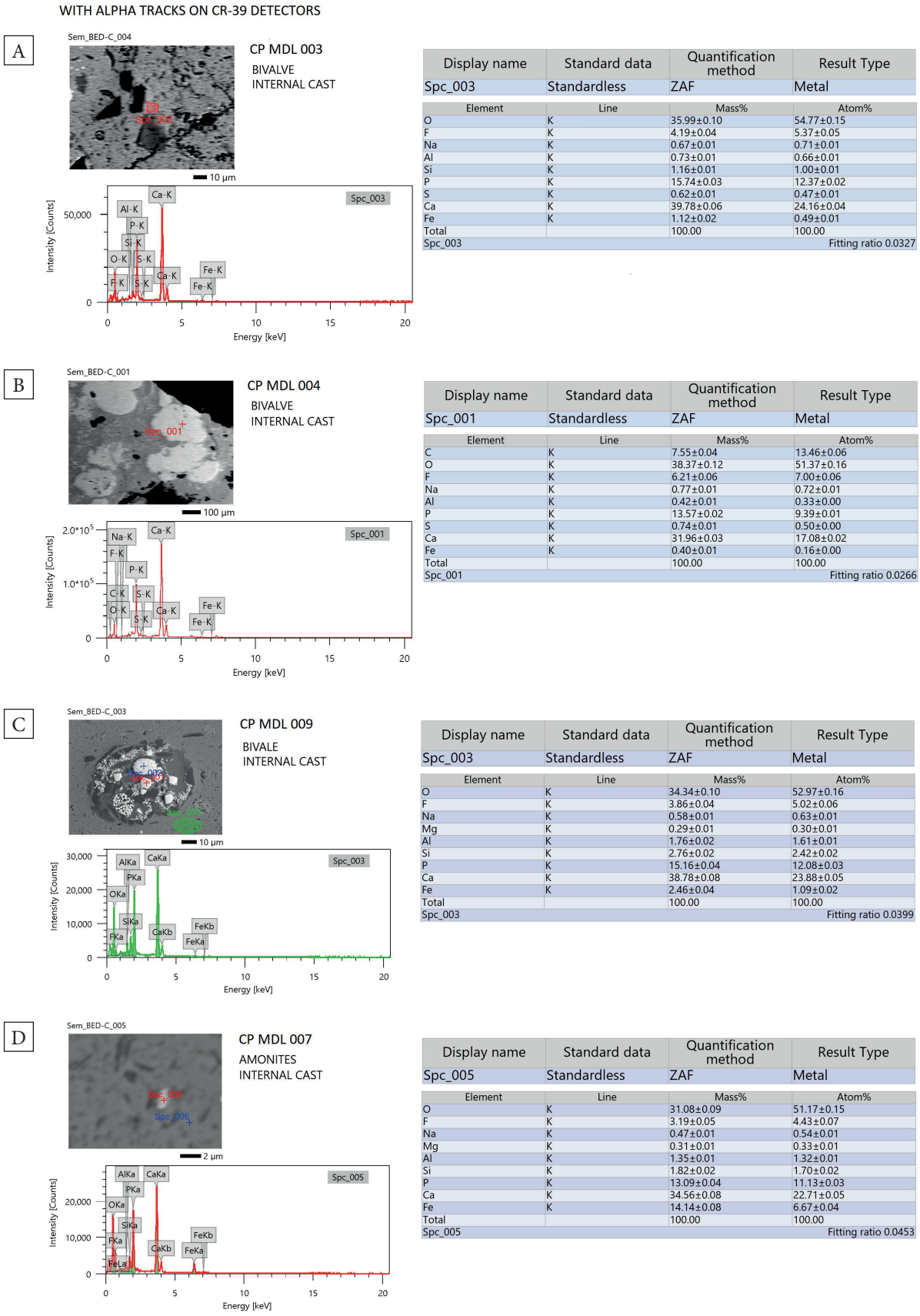

Display name	Standard data	Quantification method	Result Type
Spc_003	Standardless	ZAF	Metal

Element	Line	Mass%	Atom%
O	K	35.99±0.10	54.77±0.15
F	K	4.19±0.04	5.37±0.05
Na	K	0.67±0.01	0.71±0.01
Al	K	0.73±0.01	0.66±0.01
Si	K	1.16±0.01	1.00±0.01
P	K	15.74±0.03	12.37±0.02
S	K	0.62±0.01	0.47±0.01
Ca	K	39.78±0.06	24.16±0.04
Fe	K	1.12±0.02	0.49±0.01
Total		100.00	100.00
Spc_003			Fitting ratio 0.0327

Display name	Standard data	Quantification method	Result Type
Spc_001	Standardless	ZAF	Metal

Element	Line	Mass%	Atom%
C	K	7.55±0.04	13.46±0.06
O	K	38.37±0.12	51.37±0.16
F	K	6.21±0.06	7.00±0.06
Na	K	0.77±0.01	0.72±0.01
Al	K	0.42±0.01	0.33±0.00
P	K	13.57±0.02	9.39±0.01
S	K	0.74±0.01	0.50±0.00
Ca	K	31.96±0.03	17.08±0.02
Fe	K	0.40±0.01	0.16±0.00
Total		100.00	100.00
Spc_001			Fitting ratio 0.0266

Display name	Standard data	Quantification method	Result Type
Spc_003	Standardless	ZAF	Metal

Element	Line	Mass%	Atom%
O	K	34.34±0.10	52.97±0.16
F	K	3.86±0.04	5.02±0.06
Na	K	0.58±0.01	0.63±0.01
Mg	K	0.29±0.01	0.30±0.01
Al	K	1.76±0.02	1.61±0.01
Si	K	2.76±0.02	2.42±0.02
P	K	15.16±0.04	12.08±0.03
Ca	K	38.78±0.08	23.88±0.05
Fe	K	2.46±0.04	1.09±0.02
Total		100.00	100.00
Spc_003			Fitting ratio 0.0399

Display name	Standard data	Quantification method	Result Type
Spc_005	Standardless	ZAF	Metal

Element	Line	Mass%	Atom%
O	K	31.08±0.09	51.17±0.15
F	K	3.19±0.05	4.43±0.07
Na	K	0.47±0.01	0.54±0.01
Mg	K	0.31±0.01	0.33±0.01
Al	K	1.35±0.01	1.32±0.01
Si	K	1.82±0.02	1.70±0.02
P	K	13.09±0.04	11.13±0.03
Ca	K	34.56±0.08	22.71±0.05
Fe	K	14.14±0.08	6.67±0.04
Total		100.00	100.00
Spc_005			Fitting ratio 0.0453

Fig. 3. *The chemical compositions of regions where alpha tracks on CR-39 detectors were observed (internal structure of bivalves and ammonite) (for an explanation, see the text)*

WITHOUT ALPHA TRACKS ON CR-39 DETECTORS

A

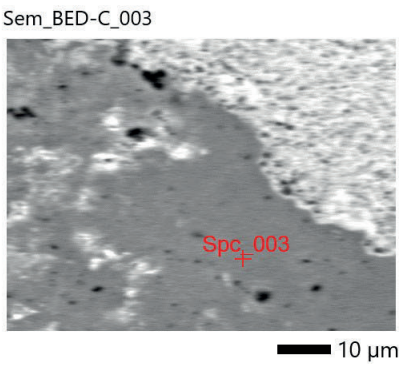

CP MDL 0001

AMMONITE
INTERNAL CAST

Display name	Standard data	Quantification method	Result Type
Spc_003	Standardless	ZAF	Metal

Element	Line	Mass%	Atom%
O	K	50.45±0.18	71.78±0.26
Mg	K	0.23±0.01	0.22±0.01
Ca	K	49.32±0.05	28.01±0.03
Total		100.00	100.00
Spc_003			Fitting ratio 0.0429

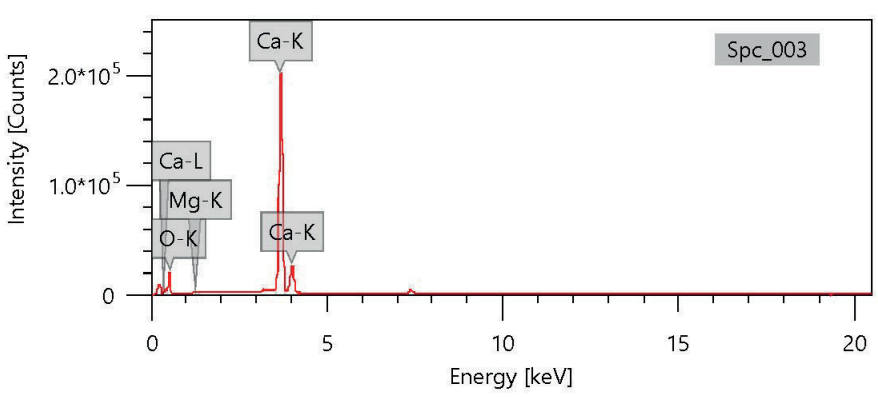

B

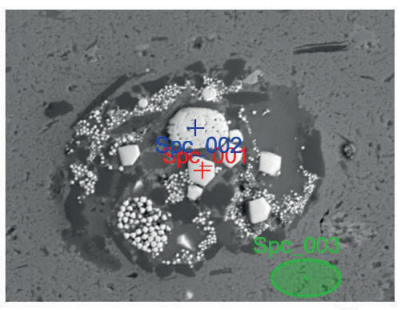

CP MDL 0009

BIVALVE
INTERNAL CAST

Display name	Standard data	Quantification method	Result Type
Spc_001	Standardless	ZAF	Metal

Element	Line	Mass%	Atom%
S	K	51.23±0.06	64.55±0.08
K	K	0.16±0.01	0.17±0.01
Ca	K	0.44±0.01	0.44±0.01
Fe	K	48.17±0.13	34.85±0.10
Total		100.00	100.00
Spc_001			Fitting ratio 0.0252

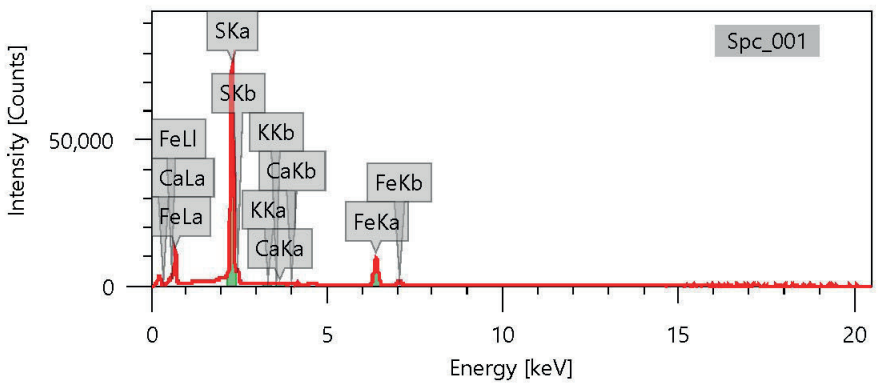

Display name	Standard data	Quantification method	Result Type
Spc_002	Standardless	ZAF	Metal

Element	Line	Mass%	Atom%
S	K	51.51±0.06	64.89±0.08
Ca	K	0.48±0.01	0.48±0.01
Fe	K	47.47±0.13	34.34±0.10
As	L	0.54±0.02	0.29±0.01
Total		100.00	100.00
Spc_002			Fitting ratio 0.0263

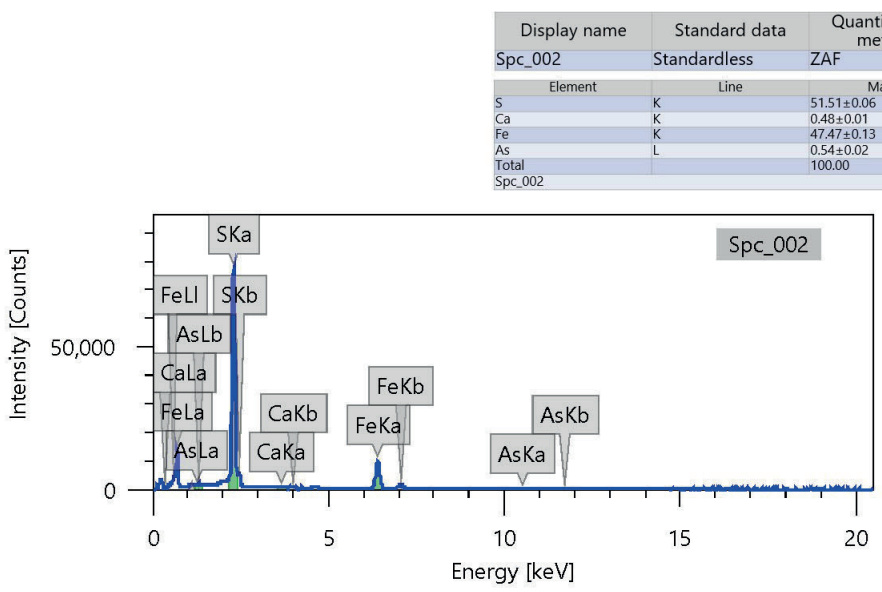

C

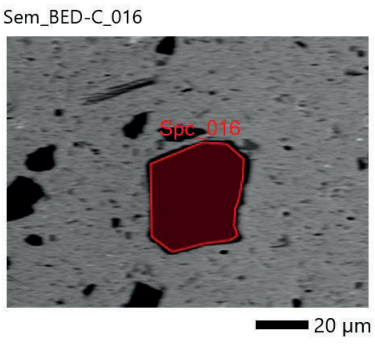

CP MDL 0003

BIVALVE
INTERNAL CAST

Display name	Standard data	Quantification method	Result Type
Spc_016	Standardless	ZAF	Metal

Element	Line	Mass%	Atom%
O	K	46.99±0.08	61.17±0.10
Si	K	50.29±0.06	37.29±0.04
P	K	0.85±0.01	0.57±0.01
Ca	K	1.87±0.02	0.97±0.01
Total		100.00	100.00
Spc_016			Fitting ratio 0.0364

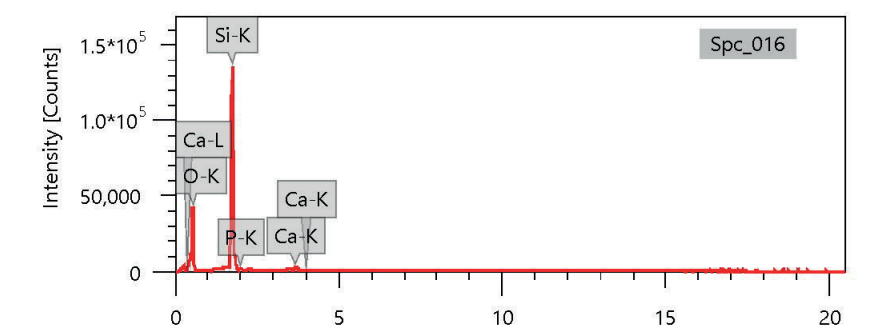

D

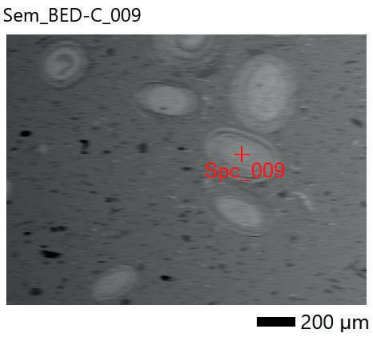

CP MDL 0007

AMMONITE
INTERNAL CAST

Display name	Standard data	Quantification method	Result Type
Spc_009	Standardless	ZAF	Metal

Element	Line	Mass%	Atom%
O	K	32.04±0.05	59.80±0.10
Mg	K	0.62±0.01	0.76±0.02
Al	K	3.18±0.02	3.52±0.03
Si	K	2.22±0.02	2.36±0.02
P	K	0.80±0.01	0.77±0.01
Ca	K	0.38±0.01	0.29±0.01
Ti	K	0.26±0.01	0.16±0.01
Fe	K	60.49±0.16	32.34±0.09
Total		100.00	100.00
Spc_009			Fitting ratio 0.0385

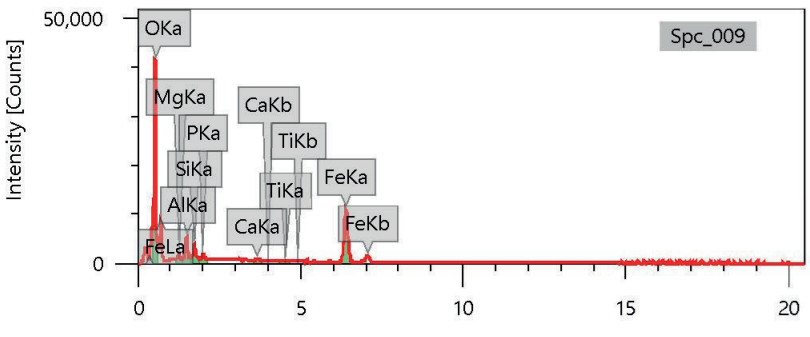

Fig. 4. *The chemical compositions of regions lacking alpha tracks on CR-39 detectors of internal casts of ammonites and bivalves (for an explanation, see the text)*

In this process, iron oxides adsorb phosphate, produced deeper in the sediment, preventing its release. Since sulphate and iron oxide reduction are sensitive to redox conditions, phosphatisation is more likely to occur in marine environments with dysoxic bottom waters (Sinha et al. 2021).

Usually, in the fossils, the apatite or carbonate-hydroxylapatite is registered. The carbonate-bearing apatite-(CaF) was found in the composition of ammonites (*Cadoceras elatmae*) of the Jurassic age from the Makar'ev South outcrop in Kostroma oblast, Russia, as minerals which replaced the soft body of ammonites (Yushkin et al. 2011). The nanocrystalline apatite (Ca-F) mineralisation was also observed in the shells of the contemporary bivalves *Lithophaga*, which shells usually contain calcium carbonate (Taylor et al. 2023). Fluorapatite is considerably less soluble and harder than calcium carbonate. It is suggested that the phosphate layer of *Lithophaga* is a functional adaptation to protect their shells from self-dissolution from their rock-dissolving glandular secretions and may also act as a defence against other shell-eroding organisms (Taylor et al. 2023). In our study, the shell of bivalve *Gryphaea dilatata* was composed of calcium carbonate; consequently, no alpha tracks were registered at the shell area (Fig. 2B). Similarly, seams visible inside the ammonites *Arietites* sp. and *Haugia variabilis* (Fig. 2A, D) were also composed of calcium carbonate (aragonite); therefore, no alpha tracks were detected in those areas. In specific conditions during diagenesis, uranium and radium elements can incorporate certain carbonate minerals such as calcite and dolomite, resulting in increased radiation in sedimentary rocks (Cole et al. 2020). This situation was not observed in our studies.

Pyrite framboids, visible in Figure 4B, can be used as a paleoenvironmental indicator. Framboids are the dominant form of pyrite in modern anoxic/suboxic environments, and they occur in both marine and freshwater environments. However, most framboids observed in nature form near the redox boundary, above the zone of bacterial sulphate reduction (Zatoń et al. 2008). Pyrites are thought to have a close connection with organic matter. Iron-framboids especially need organic-rich systems, suggesting that organics would substantially contribute to their formation (Liu et al. 2021). As the decomposition of the organic part of bivalves continues after sediment deposition through sulphate-reducing bacteria, dissolved intestinal sulphate is reduced to H_2S, which compounds with active iron to form pyrites. Meanwhile, intermediate products, H_2S and iron sulphides, also need a reduced environment, or they would be oxidatively destroyed (Taylor et al. 2023). Minerals like goethite (FeO(OH)), hematite (Fe_2O_3), and magnetite (Fe_3O_4) can adsorb uranium ions on their surfaces and concentrate uranium in specific environments (Cole et al. 2020). In our studies, the places on thin sections of fossils, composed of Fe oxides-hydroxides or iron sulphide, were devoid of radioactive elements (Fig. 4B, D).

The study reviews potential mechanisms for uranium accumulation in fossilised materials, emphasising the role of organic compounds in the surrounding sediments. These organic compounds can influence the mobility and retention of uranium through various interactions. The interaction between elements within the fossil structure and uranium depends on several processes. The preservation of organic compounds in fossils over millions of years is rare, and most fossilised material undergoes significant mineralisation and loss of original organic material. As a result, the impact of organic compounds on uranium concentration may vary depending on the fossil's age, burial conditions, and the degree of diagenetic alteration it has undergone (Aydaş et al. 2015).

The initial composition of minerals in fossils is vital because some minerals preferentially react with uranium, leading to their migration and concentration in some fossil areas. One mineral that can preferentially react with uranium is phosphate minerals, particularly apatite. Apatite is a group of phosphate minerals common in the Earth's crust that can be incorporated into the structure of fossils through fossilisation. The crystal structure of apatite contains calcium, phosphate, and hydroxide ions. Due to its chemical composition and crystal lattice, apatite has a natural affinity for uranium, and it can readily incorporate uranium ions (U^{6+}) into its structure during diagenesis and mineralisation processes. Incorporating uranium into apatite crystals can lead to elevated uranium concentrations in sedimentary rocks, fossilised bones, and other geologic formations containing apatite (Koul 1979).

Apatite is particularly important in fossilised sedimentary rocks due to its common occurrence and role in preserving uranium over geological timescales. The environment in which fossils form can affect uranium availability are lakes or other low-oxygen environments that may favour the fixation of dissolved uranium compounds, which may later accumulate in sediments. Uranium concentration can reach very high levels in specific geological settings and environments. Clay minerals, such as smectite and illite, can adsorb uranium and help retain it in sedimentary rocks (Shi et al. 2019, Philipp et al. 2022).

The organic-rich nature of black shales can create favourable conditions for uranium accumulation (Aydaş et al. 2015, Livermore et al. 2020). Organic materials like humic substances found in soils and sediments can act as chelating agents and form complexes with uranium, leading to its concentration in specific environments (Moyo et al. 2014, Zhang et al. 2020). Some organic molecules, known as ligands or chelating agents, can bind with metal ions, including uranium. Moreover, uranium can accumulate in certain sandstone formations, particularly in the form of roll-front deposits. Groundwater flowing through the porous sandstone can dissolve and transport uranium, forming uranium-rich zones. Some black shale formations can have high uranium concentrations.

In some cases, groundwater can become contaminated with high levels of uranium due to natural processes (Cole et al. 2020). For example, uranium leaching from geological can lead to elevated uranium concentrations in groundwater. Diagenetic processes, such as chemical changes and rock transformations, can affect uranium migration after fossil burial. Certain chemical reactions can promote uranium accumulation at specific locations in fossils.

CONCLUSIONS

In this research, a selection of fossil samples was analysed using CR-39 track detectors and scanning electron microscopy (SEM). The observations show that alpha emitters are almost evenly distributed throughout the fossils. No regions with concentrated tracks were identified, suggesting the absence of highly radioactive mineral grains. The uniformly distributed alpha tracks correlate with areas of mineral composition dominated by apatite, $Ca_5(PO_4)_3(Cl/F/OH)$.

The co-occurrence of phosphorus compounds and alpha emitters indicates a strong affinity of uranium for phosphorus, particularly within the former organic structures of fossilised material. Phosphorus compounds seem to be critical in absorbing uranium isotopes from the surrounding sediments. However, upon analysing the chemical composition, uranium was not detected, likely due to its concentrations being below the detection limits of EDS. Areas devoid of alpha tracks were associated with empty voids in thin sections, ooids partially composed of FeS_2 (pyrite framboids) or iron oxides (hematite), phosphorus-free regions, or other areas where microfossils partially filled internal casts.

Our research indicates that the increased radioactivity registered in some fossils is connected with phosphorous content. Small amounts of uranium are disseminated in calcium phosphate (various apatite forms). The uranium concentrations smaller than the detection limit of EDS can be successfully registered using passive track detectors.

Moreover, the study explores possible mechanisms for uranium accumulation in fossils, highlighting the influence of organic compounds and sediments that fill the fossils. These compounds can affect uranium's mobility and retention through various interactions. The interaction of uranium with elements within the fossil structure depends on multiple processes. Organic compounds rarely persist in fossils over millions of years, as fossils typically undergo significant mineralisation and lose most of their original organic content. Consequently, the extent to which organic compounds influence uranium concentration varies with the fossil's age, burial environment, and degree of diagenetic alteration.

Funding acknowledgements: This research was partially supported by funds of statutory activity to maintain the research potential of the Institute of Geological Sciences, University of Wrocław.

Declaration of interest: The authors have no conflicts of interest to declare relevant to this article's content.

Data access: The data used in this study is available on web page: https://doi.org/10.34658/RDB.BDCLHS.

REFERENCES

Aydaş C., Engin B., Kapan S., Komut T., Aydın T. & Paksu U., 2015. Dose estimation, kinetics and dating of fossil marine mollusc shells from northwestern part of Turkey. *Applied Radiation and Isotopes*, 105, 72–79. https://doi.org/10.1016/j.apradiso.2015.07.053.

Boukhenfouf W. & Boucenna A., 2012. Uranium content and dose assessment for phosphate fertiliser and soil samples: Comparison of uranium concentration between virgin soil and fertilised soil. *Radiation Protection Dosimetry*, 148(2), 263–267. https://doi.org/10.1093/rpd/ncr025.

Bruneton P., Cuney M., Dahlkamp F. & Zaluski G., 2014. *IAEA geological classification of uranium deposits*. [in:] *Uranium Raw Material for the Nuclear Fuel Cycle: Exploration, Mining, Production, Supply and Demand, Economics and Environmental Issues (URAM-2014). Summary of an International Symposium. Companion CD-ROM*, International Atomic Energy Agency, Vienna, 8–18. https://inis.iaea.org/records/78nxt-9zr16.

Cid A.S., Anjos R.M., Zamboni C.B., Cardoso R., Muniz M., Corona A., Valladares D.L., Kovacs L., Macario K., Perea D., Goso C. & Velasco H., 2014. Na, K, Ca, Mg, and U-series in fossil bone and the proposal of a radial diffusion-adsorption model of uranium uptake. *Journal of Environmental Radioactivity*, 136, 131–139. https://doi.org/10.1016/j.jenvrad.2014.05.018.

Clarkson M.O., Sweere T.C., Chiu C.F., Hennekam R., Bowyer F. & Wood R.A., 2023. Environmental controls on very high $\delta^{238}U$ values in reducing sediments: Implications for Neoproterozoic seawater records. *Earth-Science Reviews*, 237, 104306. https://doi.org/10.1016/j.earscirev.2022.104306.

Cole D.B., Planavsky N.J., Longley M., Böning P., Wilkes D., Wang X., Swanner E.D., Wittkop C., Loydell D.K., Busigny V., Knudsen A.C. & Sperling E.A., 2020. Uranium isotope fractionation in non-sulfidic anoxic settings and the global uranium isotope mass balance. *Global Biogeochemical Cycles*, 34(8), e2020GB006649. https://doi.org/10.1029/2020GB006649.

Constantin C., Popescu I.C., Oprea O. & Stoica L., 2022. U(VI) removal from diluted aqueous systems by sorption-flotation. *Scientific Reports*, 12(1), 16951. https://doi.org/10.1038/s41598-022-19002-0.

Dahl T.W., Hammarlund E.U., Rasmussen C.M.Ø., Bond D.P.G. & Canfield D.E., 2021. Sulfidic anoxia in the oceans during the Late Ordovician mass extinctions – insights from molybdenum and uranium isotopic global redox proxies. *Earth-Science Reviews*, 220, 103748. https://doi.org/10.1016/j.earscirev.2021.103748.

Deng T., Chi G., Williams-Jones A.E., Li Z., Wang Y., Xu D. & Wang Z., 2023. Re-evaluation of equilibrium relationships involving U^{6+}/U^{4+} and Fe^{3+}/Fe^{2+} in hydrothermal fluids and their implications for U mineralization. *Chemical Geology*, 625, 121432. https://doi.org/10.1016/j.chemgeo.2023.121432.

Długosz-Lisiecka M., 2016. Comparison of two spectrometric counting modes for fast analysis of selected radionuclides activity. *Journal of Radioanalytical and Nuclear Chemistry*, 309(2), 941–945. https://doi.org/10.1007/s10967-015-4688-y.

Długosz-Lisiecka M., Tyborowski D. & Krystek M., 2021. Radioactive fossils: The uranium anomaly and its paleobiological implications. *Chemosphere*, 285, 131444. https://doi.org/10.1016/j.chemosphere.2021.131444.

Hatje V., Schijf J., Johannesson K.H., Andrade R., Caetano M., Brito P., Haley B.A., Lagarde M. & Jeandel C., 2024. The global biogeochemical cycle of the rare earth elements. *Global Biogeochemical Cycles*, 38(6), e2024GB008125. https://doi.org/10.1029/2024GB008125.

Hu Z. & Gao S., 2008. Upper crustal abundances of trace elements: A revision and update. *Chemical Geology*, 253(3–4), 205–221. https://doi.org/10.1016/j.chemgeo.2008.05.010.

IAEA, 2009. *World Distribution of Uranium Deposits (UDEPO) with Uranium Deposit Classification*. IAEA-TECDOC-1629, International Atomic Energy Agency, Vienna.

Jiménez-Arroyo Á., Gabitov R., Migdisov A., Lui J., Strzelecki A., Zhao X., Guo X., Paul V., Mlsna T., Perez-Huerta A., Caporuscio F., Xu H. & Roback R., 2023. Uranium uptake by phosphate minerals at hydrothermal conditions. *Chemical Geology*, 634, 121581. https://doi.org/10.1016/j.chemgeo.2023.121581.

Koul S.L., 1979. Uranium in fossil bones. *Radiation Effects*, 43(1), 7–11. https://doi.org/10.1080/00337577908226416.

Lan Z., Wu H. & He H., 2024. Application of different radiogenic isotope systems and cyclostratigraphy in the dating of sedimentary rocks. *Earth-Science Reviews*, 250, 104695. https://doi.org/10.1016/j.earscirev.2024.104695.

Liu X., Chen X., Tostevin R., Yao H., Han K., Guo H. & Jafarian A., 2021. Post-depositional modification of carbonate ooids by sulfate-reducing bacteria: Evidence from the Lower–Middle Jurassic, Tethyan Himalayas of southern Tibet. *Sedimentary Geology*, 426, 106027. https://doi.org/10.1016/j.sedgeo.2021.106027.

Livermore B.D., Dahl T.W., Bizzarro M. & Connelly J.N., 2020. Uranium isotope compositions of biogenic carbonates – Implications for U uptake in shells and the application of the paleo-ocean oxygenation proxy. *Geochimica et Cosmochimica Acta*, 287, 50–64. https://doi.org/10.1016/j.gca.2020.07.005.

Moyo F., Tandlich R., Wilhelmi B.S. & Balaz S., 2014. Sorption of hydrophobic organic compounds on natural sorbents and organoclays from aqueous and non-aqueous solutions: A mini-review. *International Journal of Environmental Research and Public Health*, 11(5), 5020–5048. https://doi.org/10.3390/ijerph110505020.

Mustoe G.E., 2020. Uranium mineralization of fossil wood. *Geosciences*, 10(4), 133. https://doi.org/10.3390/geosciences10040133.

Ochmann A.A. & Solecki A.T., 2005. CR-39 autoradiographic micromapping of rock sections of various alpha emitters-calibration approach. *Journal of Environmental Radioactivity*, 79(2), 127–136. https://doi.org/10.1016/j.jenvrad.2004.05.017.

Philipp T., Huittinen N., Shams Aldin Azzam S., Stohr R., Stietz J., Reich T. & Schmeide K., 2022. Effect of Ca(II) on U(VI) and Np(VI) retention on Ca-bentonite and clay minerals at hyperalkaline conditions – New insights from batch sorption experiments and luminescence spectroscopy. *Science of The Total Environment*, 842, 156837. https://doi.org/10.1016/j.scitotenv.2022.156837.

Rasbury E.T., Piccione G., Holt W. & Ward W.B., 2023. Potential for constraining sequence stratigraphy and cycle stratigraphy with U-Pb dating of carbonates. *Earth-Science Reviews*, 243, 104495. https://doi.org/10.1016/j.earscirev.2023.104495.

Reynolds H.S., Ram R., Pownceby M.I., Yang Y., Chen M., Tardio J., Jones L. & Bhargava S.K., 2018. Kinetics of uranium extraction from coffinite – A comparison with other common uranium minerals. *Transactions of Nonferrous Metals Society of China*, 28(10), 2135–2142. https://doi.org/10.1016/S1003-6326(18)64858-7.

Shi Y., He J., Yang X., Zhou W., Wang J., Li X. & Liu C., 2019. Sorption of U(VI) onto natural soils and different mineral compositions: The batch method and spectroscopy analysis. *Journal of Environmental Radioactivity*, 203, 163–171. https://doi.org/10.1016/j.jenvrad.2019.03.011.

Sinha S., Muscente A.D., Schiffbauer J.D., Willimas M., Schweigert G. & Martindale R.C., 2021. Global controls on phopsphatization of fossils during the Toarcian Oceanic Anoxic Event. *Scientific Reports*, 11, 24087. https://doi.org/10.1038/s41598-021-03482-7.

Skomurski F.N., Ilton E.S., Engelhard M.H., Arey B.W. & Rosso K.M, 2011. Heterogeneous reduction of U^{6+} by structural Fe^{2+} from theory and experiment. *Geochimica et Cosmochimica Acta*, 75(22), 7277–7290. https://doi.org/10.1016/j.gca.2011.08.006.

Slukovskii Z., 2023. Uranium in lake sediments of humid zone: A case study in the Southeast Fennoscandia (Karelia, Russia). *Water*, 15(7), 1360. https://doi.org/10.3390/w15071360.

Tan X., Wang X., Chen C. & Sun A., 2007. Effect of soil humic and fulvic acids, pH and ionic strength on Th(IV) sorption to TiO_2 nanoparticles. *Applied Radiation and Isotopes*, 65(4), 375–81. https://doi.org/10.1016/j.apradiso.2006.10.014.

Taylor J.D., Glover E.A., Ball A.D. & Najorka J., 2023. Nanocrystalline fluorapatite mineralization in the calciphile rock-boring bivalve Lithophaga: functional and phylogenetic significance. *Biological Journal of the Linnean Society*, 138(2), 229–245. https://doi.org/10.1093/biolinnean/blac133.

Trueman C.N. & Tuross N., 2002. Trace elements in recent and fossil bone apatite. *Reviews in Mineralogy and Geochemistry*, 48(1), 489–521. https://doi.org/10.2138/rmg.2002.48.13.

Wang J., He B., Wei X., Li P., Liang J., Qiang S., Fan Q. & Wu W., 2019. Sorption of uranyl ions on TiO_2: Effects of pH, contact time, ionic strength, temperature and HA. *Journal of Environmental Sciences*, 75(1), 115–123. https://doi.org/10.1016/j.jes.2018.03.010.

Yushkin N.P., Katkova V.I. & Lyyurov S.V., 2011. Mineralogy of fossilized ammonites. *Geology of Ore Deposits*, 53(8), 745–750. https://doi.org/10.1134/S1075701511080174.

Zatoń M., Rakociński M. & Marynowski L., 2008. Framboidy pirytowe jako wskaźniki paleośrodowiska [Pyrite framboids as paleoenvironmental indicators]. *Przegląd Geologiczny*, 56(2), 158–164.

Zhang Y.Y., Lv J.W., Dong X.J., Fang Q., Tan W.F., Wu X.Y. & Deng Q.W., 2020. Influence on uranium(VI) migration in soil by iron and manganese salts of humic acid: Mechanism and behavior. *Environmental Pollution*, 256, 113369. https://doi.org/10.1016/j.envpol.2019.113369.

Zhao D., Wang X., Yang S., Guo Z. & Sheng G., 2012. Impact of water quality parameters on the sorption of U(VI) onto hematite. *Journal of Environmental Radioactivity*, 103(1), 20–29. https://doi.org/10.1016/j.jenvrad.2011.08.010.